

3DMA Sky Visibility Matching: An example using a simulated LEO constellation

Haosheng Xu¹, Bing Xu¹, and Li-Ta Hsu¹

¹Department of Aeronautical and Aviation Engineering, the Hong Kong Polytechnic University, Hong Kong, China

BIOGRAPHY

Haosheng Xu received the B.Sc. in Thermal Energy and Power Engineering from Jilin University, China, in 2016 and the M.Sc. at the Department of Mechanical Engineering, The Hong Kong Polytechnic University (PolyU), Hong Kong in 2019. He is studying as a Ph.D. student at the Department of Aeronautical and Aviation Engineering, PolyU. His research interests including in Context-Awareness based GNSS navigation and 3D mapping aided GNSS.

Bing Xu is currently a research assistant professor with Department of Aeronautical and Aviation Engineering, The Hong Kong Polytechnic University. Prior to the current post, he worked as a Postdoctoral Fellow in the same institute. He received his BEng and PhD degrees from Nanjing University of Science and Technology, China, in 2012 and 2018, respectively. His research focuses on signal processing with applications to the positioning system and wireless communications.

Li-Ta Hsu received the B.S. and Ph.D. degrees in aeronautics and astronautics from National Cheng Kung University, Taiwan, in 2007 and 2013, respectively. He is currently an assistant professor with the Division of Aeronautical and Aviation Engineering, Hong Kong Polytechnic University, before he served as post-doctoral researcher in Institute of Industrial Science at University of Tokyo, Japan. In 2012, he was a visiting scholar in University College London, U.K. He was a technical representative in ION in 2019-2021 and is an Associate Fellow of RIN. His research interests include GNSS positioning in challenging environments and localization for pedestrian, autonomous driving vehicle and unmanned aerial vehicle.

ABSTRACT

The Global Navigation Satellites Systems (GNSS) system is the conventional approach to provide the localization service in the urban area. However, the performance of GNSS is degraded by non-line-of-sight (NLOS) and multipath effects from the surrounding buildings. To solve this issue, the 3D building model is applied with the GNSS measurement by various matching schemes, which is called 3DMA GNSS. Recently, the geometry of the surrounding building can be estimated directly from the GNSS measurement instead of the 3D building model as sky visibility estimation, but this algorithm is limited by the number of GNSS satellites. In this paper, we developed an innovative sky visibility estimation by the SVM regression and simulated the real-time LEO constellation for the sky visibility estimation. With such improvement, the mean elevation differences between the 3D building model and our estimation is less than 10 degrees on our experiment in Hong Kong urban environment. After that, we developed sky visibility matching with the 3D building model to get the position solution. For the ideal condition, the 2D position error can be less than 1 meter in the urban canyon, and the performance of matching our estimated sky visibility also shows the potentials.

1. INTRODUCTION

Nowadays, positioning services for pedestrians are in high demand, especially in urban areas. However, the global navigation satellite systems (GNSS) performance in urban areas is degraded due to multipath and non-line-of-sight (NLOS) signals. To solve this problem, the 3D-mapping-aided (3DMA) GNSS positioning is introduced by utilizing the information of the surrounding building model. The principle of 3DMA GNSS is to match position candidates with measurements, like the satellite visibility and pseudorange, instead of finding the solution from the pseudorange measurements directly. For example, the satellite visibility can be predicted as line-of-sight (LOS) or NLOS by 3D building models. On the other hand, satellite visibility can also be classified by many approaches[1-3]. Comparing the observed and predicted satellite visibility over candidate locations, the candidates with high likelihood are considered as the solution by using a scoring scheme, which is called shadow matching[4]. Besides the satellite visibility, the pseudorange and carrier-to-noise ratio (C/N0) of the NLOS signal can be measured and predicted by ray tracing[5, 6]. The likelihood score from the estimated and measured pseudorange has been integrated into the matching scheme as the likelihood-based GNSS positioning[7, 8]. These approaches mainly use features from the GNSS

measurements for matching and considering satellites as an individual score, which is limited by the number of available GNSS measurements. Moreover, the performance of 3DMA GNSS varies in different street geometries and urban environments. For shadow matching, the root means square positioning error ranges from about 9 m to 35m with about 34% sky blockage in the London city[9].

In 3DMA GNSS, the sky visibility is used to describe the percentage of the sky from the fish-eye camera as the different levels of the urban canyon, such as slight urban, middle urban, and deep urban. In our previous work, we estimated the outline of the building boundary and derived the sky visibility [10]. The building boundary is estimated from a smoothing fitting as the elevation angles from 1° to 360° azimuth angle from the GNSS measurements. However, the accuracy of our previous sky visibility estimation is still not enough for high-precision positioning applications [10]. Because the geometrical distribution of GNSS cannot provide good coverage for some areas in the GNSS sky plot, the azimuth angle differences of two nearby LOS satellites can be more than 120° in a deep urban scenario [10], which makes the estimation inaccurate.

On the other hand, the Low Earth Orbit (LEO) satellite constellations provide us with better satellite geometries. According to the Starlink website [11], the LEO constellation of Starlink had launched around 1,800 satellites till September of 2021, with more than nearly 12,000 satellites in the next six years [12] [13]. Besides Starlink, many commercial companies planed huge LEO constellations, which makes our implementation over LEO satellites meaningful and feasible in the future. The raw measurement of LEO constellations is similar to the GNSS measurements, containing ranging measurement and satellite orbit information from the Two-Line Elements (TLE) ephemeris [14].

In this paper, an innovative method of sky visibility estimation is developed with the support vector machines (SVM) regression approach. To solve the geometry issue of estimation, the LEO satellites and GNSS satellites are implemented into our estimation together. Moreover, to evaluate the sky visibility estimation performance, we define the sky visibility as,

$$sky(az) = ele_{az} \text{ where } az = 1^\circ, 2^\circ, \dots, 360^\circ \quad (1)$$

After obtaining the sky visibility, a 3D building model-assisted positioning method is developed by matching the estimated user's sky visibility and the pre-generated sky visibility over position candidates. For the matching section, we provide two matching score schemes from the idea of matching sky visibility. Compared with shadow matching, these methods match position candidates in the dimensions of 360 and have the potential of better performance than the conventional one.

The structure of the paper is the following: The sky visibility estimation is introduced in section 2, and 3DMA sky visibility matching is introduced in section 3. In section 4, the performance of sky visibility estimation is evaluated in different scenarios. Then sky visibility matching results are evaluated in the point-wise visibility matching, and shadow matching. To explore the limitation of sky visibility matching, the real sky visibility is taken into the scoring scheme and the estimated one is tested for the real application.

2. METHODOLOGY

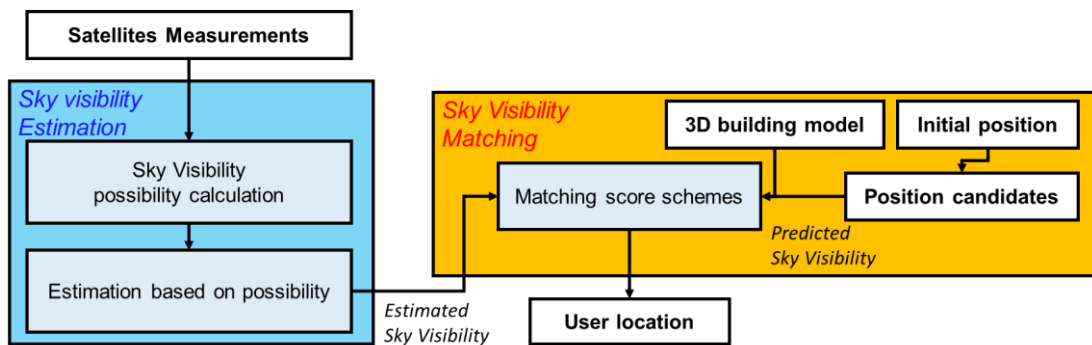


Fig. 1 Flowchart of the proposed algorithm

The flowchart of the proposed algorithm is shown in Fig. 1. We propose a 3DMA positioning algorithm with estimating the sky visibility of user location and matching it with position candidates. Firstly, the raw measurements of satellites give us satellites' azimuth angle, elevation angle, and their satellite visibilities by using some machine learning algorithms [15], then the possibility of sky visibility candidates is given by the SVM regression approach. After that, the sky visibility is derived by selecting the

candidates with high possibilities. Secondly, the 3D building model can provide the predicted sky visibility for all position candidates. Finally, the user location is calculated from the ground truth likelihood of position candidates by different matching score schemes.

2.1 Sky Visibility Estimation

In the real environment, the visibilities of satellites are categorized by the building boundary as LOS or NLOS, which is shown in Fig. 2. For the sky visibility estimation, the real building boundary is not known and needs to be estimated, but the azimuth, elevation angle of satellites can be found by using the ephemeris, and their satellite visibilities. Our estimation is to apply this information to estimate and refine the building boundary. The LOS satellite exists without any blockage, referred to as the sky area in the sky plot, while the NLOS satellite exists in the blockage area. The building boundary is the edge between these two areas. As such, sky visibility estimation is a problem of segmentation between the sky and blockage area. To solve the segmentation problem, the SVM regression is an efficient tool [16].

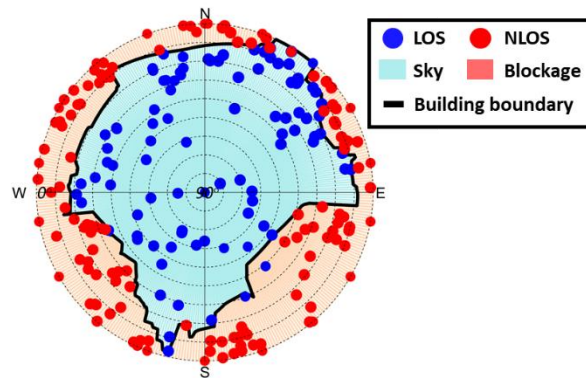


Fig. 2 Demonstration of sky and blockage in the sky plot

As the geometry of satellites, the elevation and azimuth angle of satellites can be easily computed with the ephemeris and user locations. In our assumption, the tracked satellites can be categorized from their raw measurements into two types, LOS and NLOS satellites by some classification approach. Moreover, some satellite signals are too weak to be tracked in the receiver because of the attenuation by surrounding buildings. These satellites are also categorized as NLOS satellites. The satellite categories for sky visibility estimation are shown in Table 1.

Table 1 The satellite categories for sky visibility estimation

	Satellite Type		
	Tracked & Classified		Not-tracked
Visibility	LOS	NLOS	NLOS

The visibility of satellites is defined as

$$vis_{sat}^j = \begin{cases} +1 & \text{if } j \text{ is LOS satellite} \\ -1 & \text{if } j \text{ is NLOS satellite} \end{cases} \quad (2)$$

The SVM can find the edge between two types of features in the high dimensional hyperplane by modulating the linear function,

$$y = \sum_{j=1}^m w_j x_j + b \quad (3)$$

where x is a multivariate set of m observations with response y , and the w_j is the parameter of the hyperplane vector; b is the bias. In our application, the x contains satellite azimuth and elevation angle of satellite j with the total satellites number m , and the response is the visibility of satellites vis_{sat}^j ,

$$x_j = (az_j, el_j), y_j = vis_{sat}^j \quad (4)$$

Moreover, the kernel trick is applied to reduce the computational load and improve the segment performance, the kernel function is Radial basis function kernel (RBF), which is expressed as,

$$K(\mathbf{x}, \mathbf{x}') = \exp\left(-\frac{\|\mathbf{x}-\mathbf{x}'\|_2^2}{2\sigma^2}\right) \quad (5)$$

where σ is the hyperparameter by heuristic procedure, $\|\mathbf{x}-\mathbf{x}'\|_2$ is the Euclidean distance between two feature sets. The objective function of the linear function is

$$\operatorname{argmin}\left(\frac{\|w\|^2}{2}\right) \quad (6)$$

where w is the magnitude of the normal vector, and the modeled linear function is defined as $f(x)$,

$$f(x) = \begin{bmatrix} \mathbf{w} \\ b \end{bmatrix}^T \begin{bmatrix} \mathbf{x} \\ 1 \end{bmatrix} = \mathbf{w}^T \mathbf{x} + b \quad (7)$$

After obtaining the SVM linear model $f(x)$, the SVM regression method provides the regression score as the output. This method is similar to the testing method of a machine learning process, the regression score is calculated as,

$$r = f(\mathbf{x}') \quad (8)$$

Back to our sky visibility problem, we input the regression model with sky visibility candidates, and the sky visibility candidates are expressed as,

$$\mathbf{candidates} = \begin{bmatrix} az \\ \mathbf{el}_{az} \end{bmatrix} = \mathbf{x}' \quad (9)$$

where $az = 1^\circ, 2^\circ, \dots, 360^\circ$; $\mathbf{el}_{az} \in [0^\circ, 1^\circ, \dots, 90^\circ]$, for each azimuth az , the possibility for each candidate i , is calculated by the normalizing the regression score,

$$p_{az}^i = \frac{\min(|r_{az}|) - |r_{az}^i|}{\min(|r_{az}|) - \max(|r_{az}|)} \quad (10)$$

where r_{az} is the regression score of sky visibility candidates at the azimuth angle az . Moreover, to make regression score scaling between -1 and 1, some hypothesized satellites are added in the high elevation angle of 90-degree as the LOS satellites and the low elevation angle of 0-degree as the NLOS satellites, respectively. The hypothesized satellites and sky visibility candidates with their possibility are shown in Fig. 3.

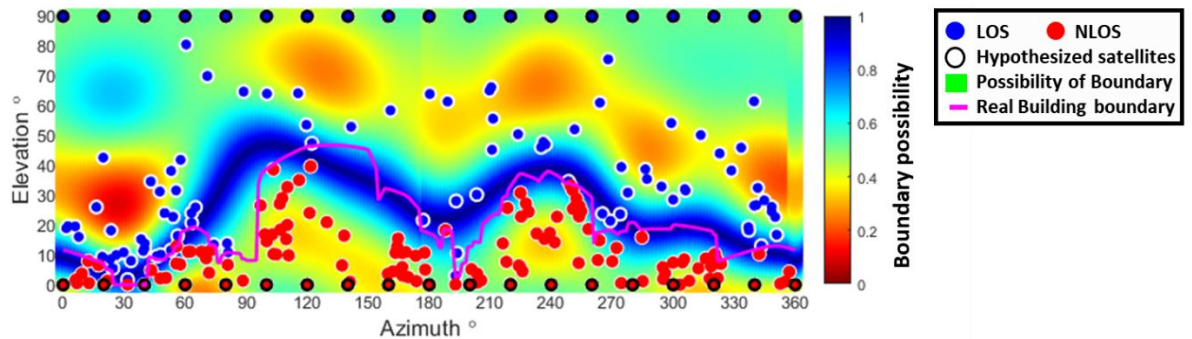


Fig. 3 Demonstration of the hypothesized satellites and sky visibility candidates with their possibilities

After that, for azimuth angle az , the elevation angle of estimated sky visibility el_{az}^{est} is calculated by:

$$el_{az}^{est} = \frac{\sum n(el_{az}^i \cdot p_{az}^i)}{\sum n p_{az}^i} | p_{az}^i \geq 0.7 \quad (11)$$

where el_{az}^i, p_{az}^i are the elevation angle and possibility of candidate i at the azimuth angle az , respectively, and the candidates are selected by the threshold of possibility larger than 70%. n is the number of selected candidates at the azimuth angle az . Finally, the estimated sky visibility can be described as

$$skv_{est}(az) = el_{az}^{est}, \text{ where } az = 1^\circ, 2^\circ, \dots, 360^\circ \quad (12)$$

An example of the estimated sky visibility is shown in Fig. 4.

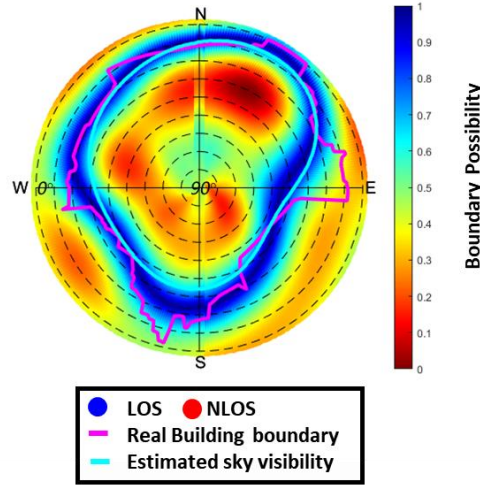


Fig. 4 An example of the estimated sky visibility

From Fig. 4, we find that the estimated sky visibility is close to the real building boundary, which is generated from the 3D building model and the ground truth of the receiver.

2.2 Sky Visibility Matching

The flowchart of sky visibility matching is shown in Fig. 5. In this algorithm, the main modules are introduced as follows:

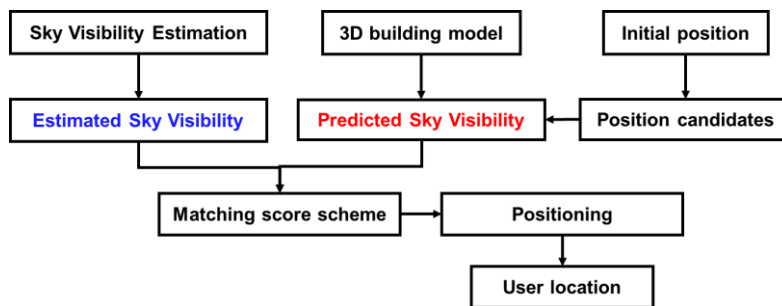


Fig. 5 Flowchart of sky visibility matching

Initial position

For conventional 3DMA positioning methods, such as shadow matching, the initial approximate solution comes from the GNSS or the other sensors [17]. Similar to shadow matching, in our algorithm, we take a National Marine Electronics Association (NMEA) solution as the initial guess. The NMEA solution is available for most commercial GNSS receivers, and its accuracy is less than 30 meters in the deep urban area according to our previous results [10].

Position candidates

The candidate particles are around the initial approximate solution, within a 50 meter by 50-meter square area with a 2-meter resolution. Additionally, the indoor particles are excluded with the help of the 3D building model, as shown in Fig. 6.

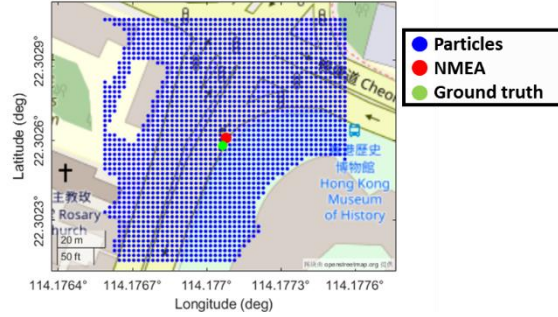


Fig. 6 Demonstration of position candidates sampling

Predicted Sky Visibility and Estimated Sky Visibility

For each particle, the predicted sky visibility is derived from the particle location and the surrounding 3D building models [18]. For each azimuth of the predicted sky visibility, the highest elevation of the surrounding building is considered as the elevation of the building boundary. The predicted sky visibility of particle i is expressed by

$$sky^i(az) = el_{az}, \text{ where } az = 1^\circ, 2^\circ, \dots, 360^\circ \quad (13)$$

The estimated sky visibility is introduced in the previous section, which comes from the receiver's measurement. We also introduce the predicted satellite visibility and estimated satellite visibility for the comparison to the shadow matching. The predicted satellite visibility is based on the predicted sky visibility. The satellites would be predicted as LOS if the elevation angle of satellites is higher than the elevation angle of sky visibility at the same azimuth, and vice versa for the NLOS satellites. The predicted satellite visibility is compared to the estimated sky visibility.

Matching Score Scheme

For the matching scheme, we designed two methods by comparing the elevation angles of the estimated sky visibility of the receiver and the predicted sky visibility of particles. The idea of the first scheme is to compare the elevation angles in each azimuth, which we call point-wise. The point-wise matching score scheme can be described as

$$s^i = \sum_{az=1}^{360} |el_{az}^i - el_{az}^{est}| \quad (14)$$

where s^i is the score of particle i . el_{az}^i and el_{az}^{est} is the elevation angle of the predicted and estimated sky visibility at the azimuth angle az . For the feature-wise approach, the elevation angles are segmented by every 60° azimuth angle. Then, the absolute mean of elevation angle difference is considered as the feature of each segment. By integrating these features, the feature-wise score would be derived.

$$s^i = \prod_{n=1}^6 |\Delta el_{60^\circ}^n| \quad (15)$$

where $\Delta el_{60^\circ}^n$ is the mean elevation angle of azimuth segment n . Because we compared the positioning performance between shadow matching and visibility matching, the scoring scheme of shadow matching is shown in Table. 2.

Table 2 Matching score scheme with satellite visibility

Matching score scheme		Predicted	
		LOS	NLOS
Tracked and classified	LOS	0	1
	NLOS	1	0
Not-tracked		\	0

Positioning

After computing matching score, the possibility of ground truth for particle i would be derived by

$$p_i = \frac{s_{max} - s^i}{s_{max} - s_{min}} \quad (16)$$

where s_{max} and s_{min} are the maximum and minimum matching scores of all particles. A threshold of 80% is set to pick the high ground truth possibility particles, then our final positioning solution is generated by taking the average of these particles. The user location in the Earth-centered, Earth-fixed (ECEF) coordinate is generated by

$$Pos = \frac{\sum_{i=1}^n [x_i \ y_i \ z_i]}{n} \mid p_i \geq 0.8 \quad (17)$$

where $[x_i \ y_i \ z_i]$ is the location of particle i in ECEF coordinate, and n is the number of the picked particles.

3. PERFORMANCE ANALYZE RESULT

Eight experiments were conducted in the different urban areas in Hong Kong and the performance of 3DMA shadow matching and sky visibility matching is evaluated. For the GNSS satellites, we used the commercial-grade receiver Ublox F9p with the constellation of GPS, GLONASS, Galileo, and BeiDou. For not-tracked GNSS satellites, their azimuth and elevation angle is calculated from the ephemeris of the reference station by Hong Kong Land Department and the rough experimental location. For the LEO satellites, the orbit parameter of LEO satellites are collected on the ‘celestrak’ website [14], and the simplified perturbations models (SGP4) model can provide enough precision in the orbit position for us [19]. The LEO constellation contains the satellites from Globalstar, Intelsat, OneWeb, Orbcomm, and Starlink. The locations of experiments and their sky plot with sky and blockage area are shown in Fig. 7.

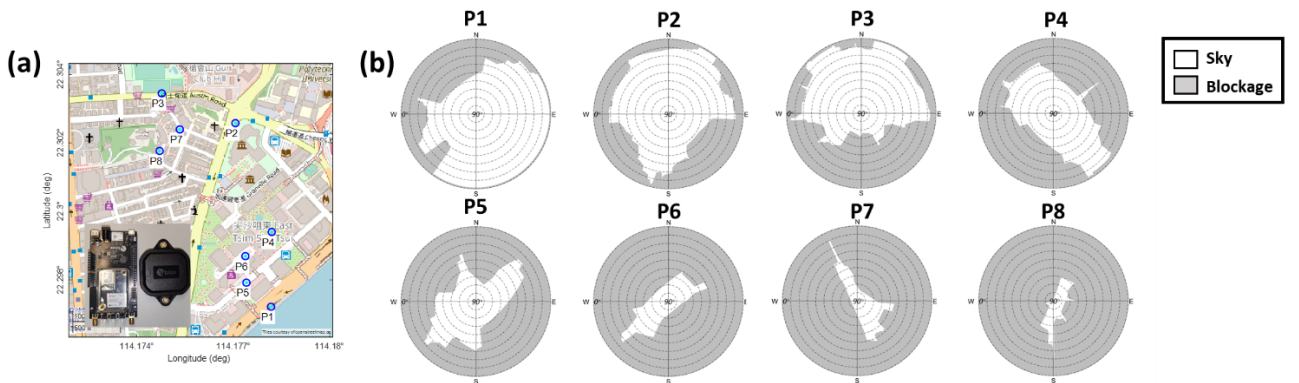


Fig. 7. (a) The receiver and locations for the data collection. (b) Sky plot of eight experimental locations with sky and blockage area

For each location, the period of GNSS measurement is 15 minutes, and every four experiments are collected at the same time. The orbit of the LEO satellites is calculated with the same received time of GNSS measurement as the real-time, and the number of satellites in the LEO and GNSS Constellation is shown in Table. 3. For the GNSS constellation, the total number is the number of satellites that can be received in the open sky, and the received number is the recorded satellite number from the Rinex file.

Table 3 Mean of number from LEO and GNSS constellation

Period	Location	LEO Constellation	GNSS Constellation	
		/	Total	Received
I	1	192.71	34.00	21.42
	4			26.35
	5			23.59
	6			19.32
II	2	173.72	45.57	26.35
	3			23.59
	7			19.32
	8			19.56

For the evaluation of results, the performance of sky visibility estimation is introduced at first, then the performance of sky visibility matching is compared with the shadow matching.

3.1 The Performance of sky visibility estimation

In this experiment, the evaluation contains two parts, including sky visibility estimation with the GNSS constellation and the GNSS + LEO constellation. From Table 3, we can find the number of the LEO constellation, which is available from ephemeris in Hong Kong, is nearly from 170 to 190 in two short periods. However, the number of GNSS is not larger than 50 satellites at the same time, which means the LEO constellation gives us a better satellites geometry. However, the benefit of increasing satellite number and better geometry on the sky visibility is unknown to us. In this section, we show this benefit in detail, and what should be noticed is the visibility of the satellite is based on its real environment according to the 3D building model and ground truth of location. The sky visibility estimation error based on real satellite visibility with the GNSS constellation is shown in Table 4.

Table 4. The sky visibility estimation error based on real satellite visibility with the GNSS constellation. (Unit: degree)

Location	Mean	STD	Min	Max
1	10.77	5.79	0.09	26.11
2	9.24	5.78	0.10	30.23
3	11.68	7.69	0.07	42.59
4	11.11	7.36	0.08	41.52
5	13.03	9.82	0.09	42.86
6	8.82	6.79	0.07	37.73
7	13.04	7.43	0.16	41.03
8	11.25	6.75	0.13	26.13

The estimated sky visibilities from the GNSS constellation in 8 locations are shown in Fig. 8.

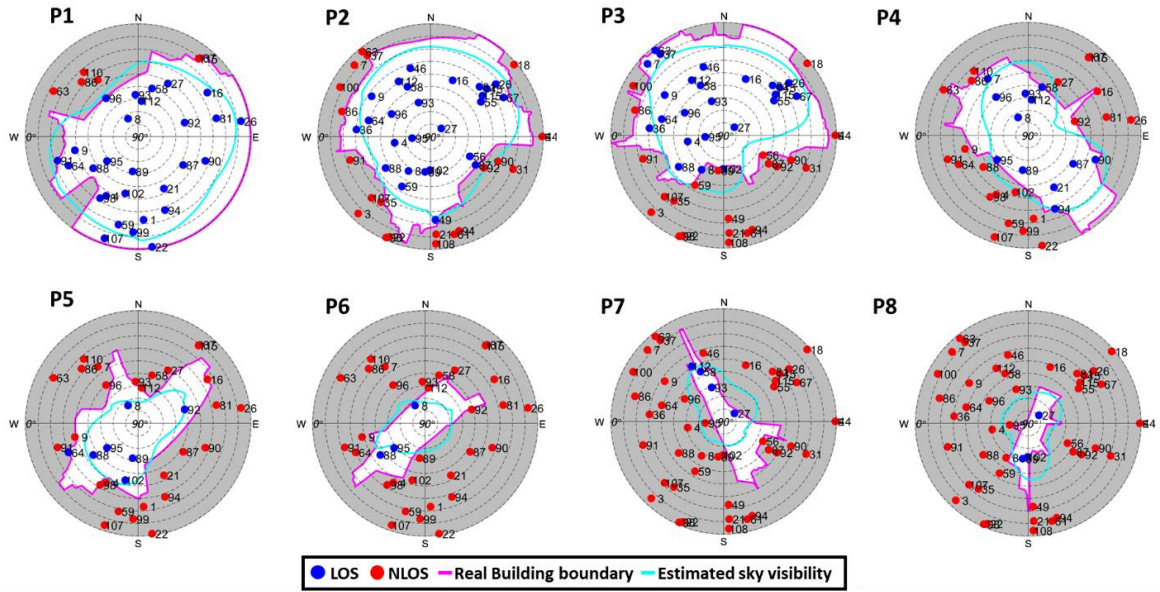


Fig. 8. Demonstration of the estimated sky visibility from the GNSS constellation.

From the estimation results in Table 4, we can find the geometry of our sky visibility is near to the real building boundary, but the mean estimation errors for all locations are around 10 degrees. The maximum value of estimation error in some azimuth can be nearly from 30 to 40 degrees. The main reason for these results can be explained by Fig.9. From Fig 9, we find the geometry of satellites is not good enough for our estimation. In many azimuths, the elevation of GNSS satellites is far away from the elevation of building boundary or even not satellite here. Our regression method estimated the boundary by the whole satellite geometry, which can still generate sky visibility for these azimuths, but this lack in satellites geometry can not provide us with the exact information about the real building boundary. For such estimation results, the potential application is not to detect the level of urban just as what we did in the previous paper [10] instead of applying it in the positioning approach. To solve the satellite geometry issue, the LEO constellation is integrated with the GNSS constellation, the sky visibility estimation error based on real satellite visibility with the GNSS+LEO constellation is shown in Table 5.

Table 5. The sky visibility estimation error based on real satellite visibility with the GNSS+LEO constellation. (Unit: degree)

Location	Mean	STD	Min	Max
1	5.32	5.45	0.07	27.76
2	4.60	4.49	0.02	24.88
3	6.56	6.28	0.02	32.47
4	6.04	5.27	0.03	32.12
5	8.05	6.17	0.04	31.54
6	6.22	5.16	0.03	25.92
7	8.59	6.65	0.05	35.31
8	8.69	5.59	0.06	29.50

The estimated sky visibilities from the GNSS +LEO constellation in 8 locations are shown in Fig. 9.

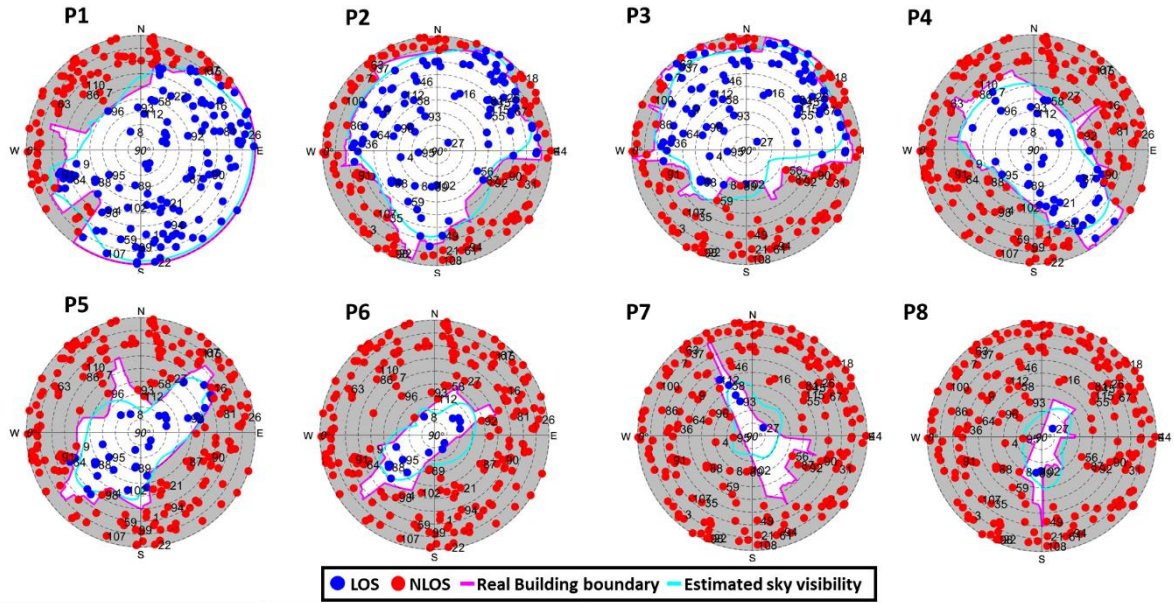


Fig. 9. Demonstration of the estimated sky visibility from the GNSS+LEO constellation.

From the estimation results in Table 5, the mean of estimation error in all locations is nearly from 5 degrees to 9 degrees, and the maximum values of estimation error are nearly 30 degrees. A clear comparison is shown in Fig 10. The GNSS geometry between Fig 9 and Fig 10 is the same, but the estimated sky visibility with the GNSS+LEO constellation is closer to the real building boundary than the one with the GNSS constellation. The estimation error is slight when there are enough satellites around the building boundary, likes the cases in P1 and P2. Meanwhile, the estimation error is large when there are no or few satellites around the building boundary. For example, in the cases in P7 and P8, there is no LOS satellite in many azimuths angle, which makes the estimation not aware of sky area from LOS satellite and the imperfect estimation. These results show that the accuracy of our estimation is mainly affected by the geometry of satellites, and the LEO constellation is a good supplement.

3.2 The Performance of sky visibility matching

To verify the performance of sky visibility matching, we separate the evaluation based on SDM, Point-wise, and Feature-wise respectively.

SDM: The algorithm of shadow matching

Point-wise: The proposed sky visibility matching with the point-wise matching score scheme

Feature-wise: The proposed sky visibility matching with the feature-wise matching score scheme

The sky visibility matching is compared with the shadow matching in the ground truth to test the best performance of each algorithm. For shadow matching, the satellites are categorized as LOS and NLOS by the ground truth of the user and the 3D building model. For sky visibility matching, the estimated sky visibility is the same as the predicted sky visibility of ground truth location, and the estimated sky visibility is fixed since the experiment is static. The positioning results of all experiments are summarized in Table 6 and Table 7.

Table 6. The mean error of different positioning approaches with ground truth (Unit: meter)

Location	SDM	Point-wise	Feature-wise
1	17.97	8.46	4.88
2	8.01	2.45	1.98
3	7.90	8.39	3.50
4	5.84	1.08	0.48
5	2.11	0.99	0.99

6	4.22	0.36	0.52
7	5.02	1.42	1.52
8	23.09	26.50	21.84

Table 7. The standard deviation of different positioning approaches with ground truth (Unit: meter)

Location	SDM	Point-wise	Feature-wise
1	4.20	0.05	0.00
2	3.76	0.03	0.00
3	2.33	0.03	0.03
4	3.80	0.11	0.00
5	1.15	0.04	0.27
6	2.81	0.07	0.01
7	3.20	0.00	0.07
8	3.56	1.42	5.48

From the tables, we can find two methods of sky visibility matching have better performance than shadow matching in most cases. The mean error of sky visibility matching with two methods is less than 1 meter in P6 and P7, while the error of shadow matching is 2.11 and 4.22 meters. Comparing the point-wise and feature-wise, the feature-wise approach has the better performance. The main reason for this is the feature-wise particles with the high ground truth possibility are more congregated around the ground truth than the point-wise ones. The ground truth possibility heatmap in P1 is shown in Fig 10. Similar improvement can be noticed in P2, P4, P5, P6, and P7.

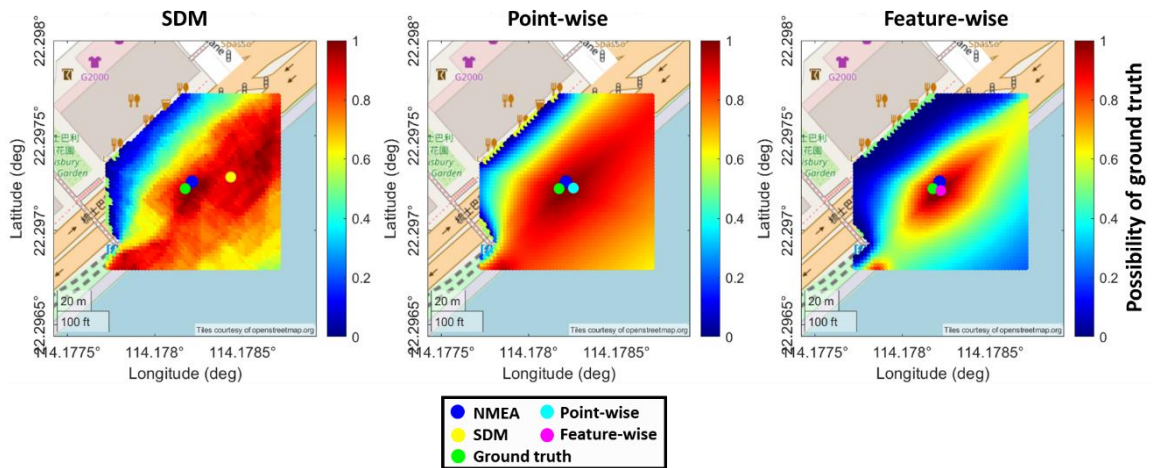


Fig. 10. Demonstration of the ground truth possibility heatmap in P1.

Moreover, we can notice the point-wise approach has a slightly larger error than the shadow matching in P3. The main reason for this is the north-side environment of P3 is an open-sky area as a small park, which makes the elevation angle of the building boundary is very low and similar in the nearby particles in the north as shown in Fig11. Furthermore, the similarity of the environment makes the ground truth possibility evenly, which can be seen in the heatmap of P3, as shown in Fig 11. Since the feature-wise approach integrates the features of each azimuth range, the impact from the similarity of the environment has been eliminated a lot with the better positioning performance.

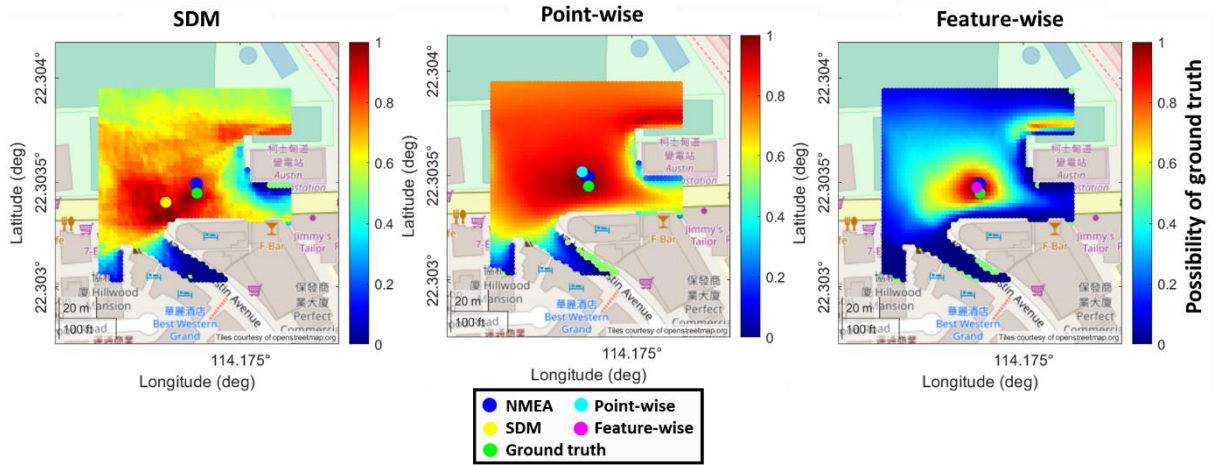


Fig. 11. Demonstration of the ground truth possibility heatmap in P3.

However, the positioning performance of P8, which is the deepest urban canyon of all locations, is far from satisfactory. The mean error of SDM, point-wise, and feature-wise is 23.09, 26.50, and 21.84 meters. From the heatmap of ground truth possibility, the main reason is many particles have similar building boundaries in the searching area, as the local minimum. In addition, we obtain the positioning solution from the average location with high possibility particles, which bring the local minimum into our final results. Demonstration of the ground truth possibility heatmap is shown in Fig. 12.

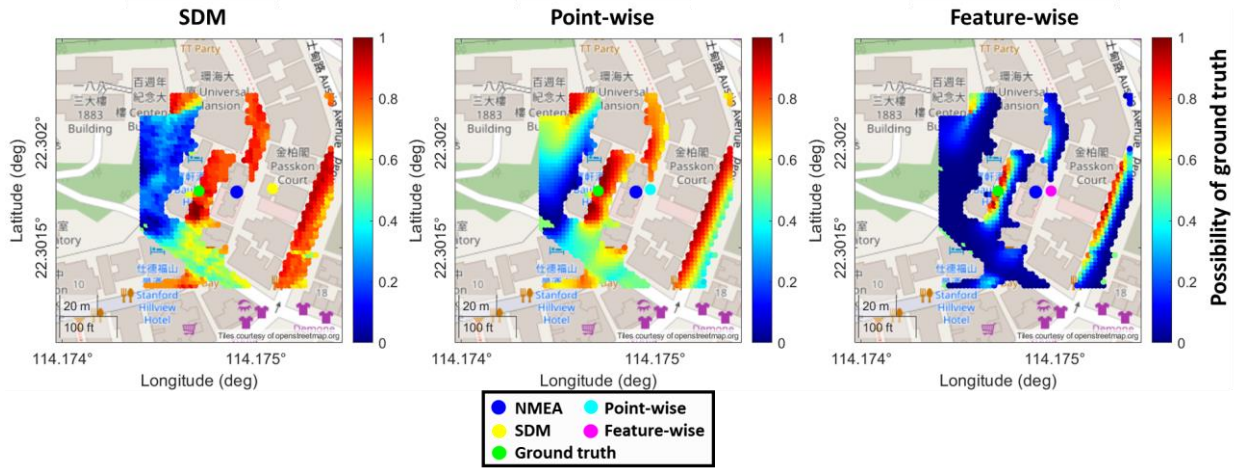


Fig. 12. Demonstration of the ground truth possibility heatmap in P8.

Since we can obtain the sky visibility based on our estimation, the sky visibility matching is compared with the shadow matching by estimated sky visibility for realistic application. The positioning results of all experiments are summarized in Table 8 and Table 9.

Table 8. The mean error of different positioning approaches with estimation (Unit: meter)

Location	SDM	Point-wise	Feature-wise
1	17.88	20.91	17.72
2	8.04	5.23	6.39
3	7.84	12.24	11.48
4	5.98	5.41	10.20
5	2.13	4.16	4.67
6	4.28	4.24	4.90

7	5.01	11.55	11.55
8	23.12	52.96	44.93

Table 9. The standard deviation of different positioning approaches with estimation (Unit: meter)

Location	SDM	Point-wise	Feature-wise
1	4.20	2.70	7.40
2	3.76	3.16	3.78
3	2.33	6.80	5.47
4	3.80	3.19	7.32
5	1.15	2.30	3.05
6	2.81	2.99	3.83
7	3.20	5.25	5.52
8	3.56	6.96	19.33

From the results, the performance of sky visibility matching is worse than the shadow matching in most locations. From the experiments in the setting of ground truth, we confirm that with more accurate features to match, the positioning performance is improved a lot. In this realistic setting, our sky visibility estimation is still far from perfect, which brings many inaccurate features into matching. Many details in the sky visibility estimation are missed and estimation varies a lot by the movement of satellites. An extreme example is in the deep urban. In P8, there are few LOS satellites are put into sky visibility estimation, the estimated sky visibility is very rough, and exists much error as shown in Fig. 13.

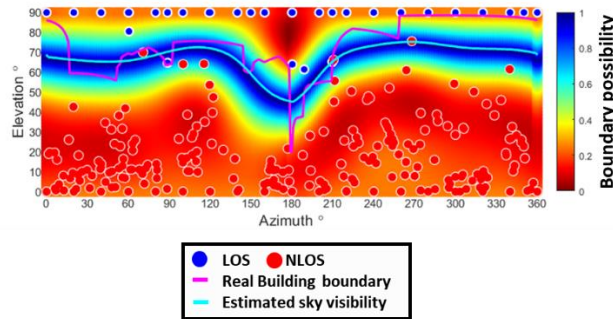


Fig. 13. Demonstration of estimated sky visibility in P8.

when we put this estimation into the matching scheme, the final results are affected by the inaccurately-estimated sky visibility and the local minimum at the same time. The ground truth possibility heatmap by estimated sky visibility is shown in Fig. 14. In this way, the evaluation of sky visibility estimation may be considered into the sky visibility matching scheme to exclude the inaccurate samples in the future, and the visibility of satellites can be designed for the matching to combine the benefit of shadow matching and sky visibility matching.

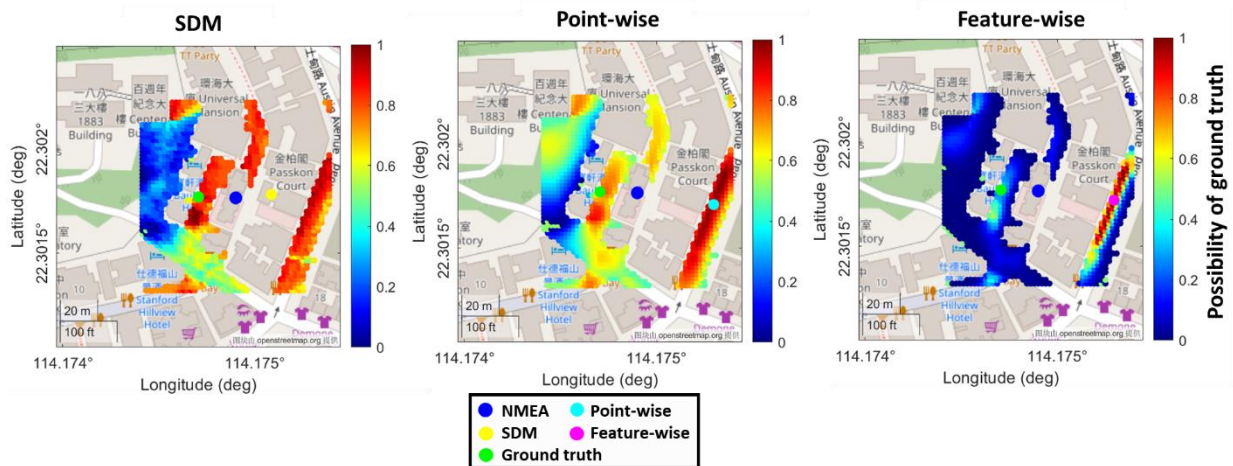


Fig. 14. Demonstration of ground truth possibility heatmap by estimated sky visibility in P8.

The sky visibility matching has shown that it can perform well in the urban area with accurate sky visibility estimation in most urban experiments. The mean positioning error of sky visibility matching with point-wise is less than 10 meters in most cases, while the mean positioning error of sky visibility matching with feature-wise is less than 5 meters. With our realistic application, the sky visibility matching is affected by the inaccurate sky visibility estimation and local minimum, which have the potential to be improved.

4. CONCLUSIONS AND FUTURE WORKS

To conclude, this study proposes to bring the 3DMA GNSS integrated with the sky visibility estimation for the urban environment application. An innovative sky visibility estimation method is developed with SVM regression, and the results show that satellite geometry is important to sky visibility estimation. The LEO constellation is simulated to assist the sky visibility estimation. The mean estimation error for the various urban canyon is less than 10 degrees. For positioning applications, we design two methods, point-wise and feature-wise matching schemes to match the ground truth candidates. Compared with shadow matching, the sky visibility matching has improved for all urban cases in the accurate sky visibility, with less than 5 meters 2D-error. Our current sky visibility estimation has also shown the accuracy of sky visibility estimation is the key part of sky visibility matching.

In the near future, the sky visibility estimation method would be developed and improved. Furthermore, the performance of sky visibility estimation would be tested in no-perfect LOS/NLOS conditions, and the matching scheme of sky visibility matching would consider the available sample of estimated sky visibility to mitigate the effects of misestimation.

REFERENCES

1. Hsu, L.T., Y. Gu, and S. Kamijo, *NLOS Correction/Exclusion for GNSS Measurement Using RAIM and City Building Models*. Sensors (Basel), 2015. **15**(7): p. 17329-49.
2. Yozevitch, R., B.B. Moshe, and A. Weissman, *A Robust GNSS LOS/NLOS Signal Classifier*. Navigation, 2016. **63**(4): p. 429-442.
3. Xu, et al., *Intelligent GPS L1 LOS/Multipath/NLOS Classifiers Based on Correlator-, RINEX- and NMEA-Level Measurements*. Remote Sensing, 2019. **11**(16).
4. Groves, P.D., *Shadow matching: a new GNSS positioning technique for urban canyons*. Journal of Navigation, 2011. **64**(3): p. 417-430.
5. Gowdayyanadoddi, N.S., et al., *A Ray-Tracing Technique to Characterize GPS Multipath in the Frequency Domain*. International Journal of Navigation and Observation, 2015. **2015**: p. 1-16.
6. Gegout, P., et al., *Ray-Tracing of GNSS Signal Through the Atmosphere Powered by CUDA, HMPP and GPUs Technologies*. IEEE Journal of Selected Topics in Applied Earth Observations and Remote Sensing, 2014. **7**(5): p. 1592-1602.
7. Groves, P.D. and M. Adjrjad, *Likelihood-based GNSS positioning using LOS/NLOS predictions from 3D mapping and pseudoranges*. GPS Solutions, 2017. **21**(4): p. 1805-1816.
8. Adjrjad, M. and P.D. Groves, *Intelligent Urban Positioning: Integration of Shadow Matching with 3D-Mapping-Aided GNSS Ranging*. Journal of Navigation, 2018. **71**(1): p. 1-20.

9. Adjrad, M., et al., *Performance assessment of 3D mapping aided GNSS part 2: Environment and mapping*. Navigation, 2019. **66**(2): p. 363-383.
10. Xu, H., et al., *Sky visibility estimation based on GNSS satellite visibility: an approach of GNSS-based context awareness*. GPS Solutions, 2020. **24**(2).
11. Starlink. <https://www.starlink.com/>. 2021. [cited 2021 Oct.1]
12. Wikipedia. <https://en.wikipedia.org/wiki/Starlink>. 2021 [cited 2021 Oct,1].
13. Cakaj, S., *The Parameters Comparison of the "Starlink" LEO Satellites Constellation for Different Orbital Shells*. Frontiers in Communications and Networks, 2021. **2**(7).
14. Kelso, T.S. <https://celestrak.com/>. 2021 [cited 2021 Oct.1].
15. Xu, H., et al., *Machine learning based LOS/NLOS classifier and robust estimator for GNSS shadow matching*. Satellite Navigation, 2020. **1**(1): p. 15.
16. Vapnik, V.N., *The Nature of Statistical Learning Theory (Second Edition)*. 2000, New York: Springer.
17. Groves, P.W., L; Adjrad, M; Ellul, C; . *GNSS Shadow Matching: The Challenges Ahead*. in *the 28th International Technical Meeting of The Satellite Division of the Institute of Navigation (ION GNSS+ 2015)*. 2015. Tampa, Florida, USA.: The Institute of Navigation.
18. Ng, H.F. and L.T. Hsu, *3D Mapping Database-Aided GNSS RTK and Its Assessments in Urban Canyons*. IEEE Transactions on Aerospace and Electronic Systems, 2021. **57**(5): p. 3150-3166.
19. Aida, S. and M. Kirschner, *Accuracy Assessment of SGP4 Orbit Information Conversion into Osculating Elements*, in *Sixth European Conference on Space Debris, ESA/ESOC*. 2013: Darmstadt, Germany. p. 22–25.